Astron. Astrophys. 321, 724–732 (1997)

ASTRONOMY
AND
ASTROPHYSICS

Stellar systems following the $R^{1/m}$ luminosity law

II. Anisotropy, velocity profiles, and the fundamental plane of elliptical galaxies

L. Ciotti[1] **and B. Lanzoni**[2]
[1]Osservatorio Astronomico di Bologna, via Zamboni 33, I-40126 Bologna, Italy
[2]Dipartimento di Astronomia, Università di Bologna, Via Zamboni 33, I-40126 Bologna, Italy

Received 11 June 1996 / Accepted 29 October 1996

Abstract. Following a first paper on this subject (Ciotti 1991, hereafter Paper I), we study the dynamical properties of spherical galaxies with surface luminosity profile described by the $R^{1/m}$-law, in which a variable degree of orbital anisotropy is allowed. The parameter m for the present models covers the range $[1, 10]$. For these models we study the self-consistently generated phase-space distribution function (DF), and we derive – as a function of m – the minimum value of the anisotropy radius for the model consistency (i.e., in order to have a nowhere negative DF). Then we study the region in the parameter space where the $R^{1/m}$ models are likely to be stable against radial-orbit instability, and we compare its size with that of the larger region corresponding to the consistency requirement. For stable anisotropic models the spatial and projected velocity dispersion profiles are obtained solving the Jeans equation, and compared to those of the globally isotropic case, already discussed in Paper I. The relevance of the results in connection with the fundamental plane (FP) of elliptical galaxies is pointed out: the effect on the projected velocity dispersion due to the maximum orbital anisotropy allowed by the stability requirement is well within the FP thickness, and so no fine-tuning for anisotropy is required. Finally, the velocity profiles are constructed as a function of the projected radius and for various degrees of anisotropy, and their deviations from a gaussian discussed.

Key words: galaxies: elliptical – galaxies: kinematics and dynamics – galaxies: structure

1. Introduction

The $R^{1/4}$-law [Eq. (1) below, with m = 4] was introduced by de Vaucouleurs (1948) to describe the projected luminosity density (or surface brightness) $I(R)$ of elliptical galaxies, and has worked remarkably well. It has no *free parameters* and depends on two well defined *physical scales*: a characteristic linear scale, $R_{\rm e}$, and a surface brightness factor, $I_\circ$.

A natural generalization of this empirical law was first proposed by Sersic (1968), as the $R^{1/m}$-law. From an observational point of view, the $R^{1/m}$-law has been widely used (see, e.g., Davies et al. 1988; Capaccioli 1989; Makino et al. 1990; Young & Currie 1994; Andredakis, Peletier & Balcells 1995; Courteau, de Jong & Broeils 1996). In particular, for normal ellipticals and brightest cluster galaxies, a correlation between their luminosity L and the value of m has been found, in the direction of m increasing with increasing L (Caon, Capaccioli & D'Onofrio 1993; Graham et al. 1996).

From a theoretical point of view much less work has been done on the $R^{1/m}$-law, its apparent universality, and its possible applications to the problem of the FP of elliptical galaxies (Djorgovski & Davis 1987; Dressler et al. 1987; Bender, Burstein & Faber 1992) and only *one-component, spherically symmetric, globally isotropic models* have been studied (Paper I; Hjorth & Madsen 1991; Ciotti, Lanzoni & Renzini 1996; Graham & Colless 1996). Considering the extensive use of the $R^{1/m}$-law we plan to extend the investigation of this class of models.

The interest in the study of the dynamical properties of the $R^{1/m}$ models is also renewed following recent ground based observations (Møller, Stiavelli, & Zeilinger 1995), and Hubble Space Telescope ones, showing that the spatial luminosity distributions of elliptical galaxies approach the power-law form $\rho(r) \propto r^{-\gamma}$ at small radii, with $0 \leq \gamma \leq 2.5$ (Crane et al. 1993; Jaffe et al. 1994; Ferrarese et al. 1994; Lauer et al. 1995; Kormendy et al. 1995; Byun et al. 1996; de Zeeuw & Carollo 1996). Since the deprojected density of the $R^{1/m}$ models increases toward the center as $r^{-(m-1)/m}$ for $m > 1$ (Paper I), this family of models can be used to study power-law galaxies with $0 < \gamma < 1$.

In particular, in this paper we study one-component, spherically symmetric, anisotropic $R^{1/m}$ models, in which orbital anisotropy follows the widely used OM parameterization (Osipkov 1979, Merritt 1985). We numerically construct their phase-space DF, and we determine the region in the parameter space where anisotropic $R^{1/m}$ models are consistent, i.e., their DF is

Send offprint requests to: L. Ciotti; e-mail ciotti@astbo3.bo.astro.it

positive over all the accessible phase-space. We then investigate the models stability against radial orbit instability, by using the global stability parameter, comparing the radial and tangential kinetic energies. In this way we approximately bound the region in the parameter space where the anisotropic models are consistent but (with high probability) unstable.

Having determined the region in the parameter space where the $R^{1/m}$ models are physical, we study their main properties. First of all the spatial and projected velocity dispersions are derived and discussed. Then we construct their velocity profiles (hereafter VPs), and fit them using the Gauss-Hermite series, discussing their deviations from a pure gaussian for different m and anisotropies.

In a third paper (Paper III, Ciotti & Lanzoni 1996) we study in detail the properties of the DF, VPs, and velocity dispersion profiles of two-component spherically symmetric $R^{1/m}$ models, in order to understand how the superposition of a dark matter halo modifies the internal dynamics of the models and their observational properties.

The paper is organized as follows. In Sect. 2 the basic properties of the $R^{1/m}$ models, already discussed in Paper I, are summarized. In Sect. 3 the DFs for anisotropic models are derived and discussed, together with the limits imposed on orbital anisotropy for the models consistency and stability. In Sect. 4 we obtain the velocity dispersion profiles of some characteristic models, and some observationally interesting properties are presented. A short discussion on the implications of the obtained results on the problem of the FP of ellipticals is given. In Sect. 5 the models VPs are constructed, and then fitted using the Gauss-Hermite series, thus quantifying the departures from gaussianity. Finally in Sect. 6 the main conclusions are summarized.

2. A summary of the properties of spherical $R^{1/m}$ models

Here we give a short summary of the basic properties of the $R^{1/m}$ models, as derived in Paper I. A full treatment is given there, and we will refer to equations in that paper as Eq. (P#).

The spherical $R^{1/m}$ models are defined as a one-parameter family of stationary stellar systems, with surface brightness profile given by

$$I(R) = I_\circ \exp(-b\eta^{1/m}), \tag{1}$$

where $I_\circ$ is the central surface brightness, $\eta \equiv R/R_\mathrm{e}$, R is the projected radius, and R_e is the *effective radius* (i.e. the projected radius inside which the projected luminosity equals half of the total luminosity). The defining parameter is m, a positive real number, and b is a dimensionless parameter whose value is determined by the definition of R_e. The function $b = b(m)$ [Eq. (P5)] is very well fitted by the linear interpolation $b(m) = 2m - 0.324$, for $0.5 \leq m \leq 10$, with relative errors smaller than 0.001, and $b(4) = 7.66924944$ (Paper I). The total luminosity L_m is given by $L_m = I_\circ R_\mathrm{e}^2 \times \widetilde{L}_m$, with

$$\widetilde{L}_m = \frac{2\pi m}{b^{2m}}\Gamma(2m), \tag{2}$$

where Γ is the complete gamma function [Eq. (P4), Erdély, Magnus, Oberhettinger & Tricomi 1953, hereafter EMOT, vol. I, p. 1].

The most important deprojected quantity associated to $I(R)$ is the *luminosity density* ν, which is related to the mass density via $\rho(r) = \Upsilon\nu(r)$, where Υ is the mass-to-light ratio, and r is the spatial radius. We assume a constant Υ, so that the main quantities (mass inside r, potential, velocity dispersion, etc.) depend only on the luminosity density $\nu(r)$, which is related to the surface brightness profile by an Abel integral equation (see, e.g., Binney & Tremaine 1987, hereafter BT):

$$\nu(r) = -\frac{1}{\pi}\left[\int_r^\infty \frac{dI}{dR}\frac{dR}{\sqrt{R^2-r^2}} - \lim_{R\to\infty}\frac{I(R)}{\sqrt{R^2-r^2}}\right]. \tag{3}$$

The second term in the r.h.s. of Eq. (3) is zero for any positive value of m, and the resulting luminosity density $\nu_m(r) = (I_\circ/R_\mathrm{e}) \times \widetilde{\nu}_m(s)$, where $s \equiv r/R_\mathrm{e}$, is extensively discussed in Paper I. The asymptotic behaviour of $\widetilde{\nu}_m$ for $r \to \infty$ is given in Eq. (P8), while for $r \to 0$ one obtains:

$$\widetilde{\nu}_m(0) = \frac{b^m}{\pi}\Gamma(1-m), \qquad m < 1 \tag{4}$$

$$\widetilde{\nu}_m(s) \sim \frac{b}{\pi}\ln\left(\frac{2}{bs}\right), \qquad m = 1 \tag{5}$$

$$\widetilde{\nu}_m(s) \sim \frac{B[1/2,(m-1)/2m]}{2mb^{m-1}}\exp(-bs^{1/m})s^{(1-m)/m}, \tag{6}$$

for $m > 1$, and where $B(x,y)$ is the complete beta function [Eqs. (P9)-(PA5), EMOT, vol. I, p. 9]. It should be noted that for $m > 1$ the density diverges at the origin as $r^{(1-m)/m}$; therefore the divergence is worse for higher-m models. Finally, as in Paper I, we consider the *relative* potential $\psi_m(r) = G\Upsilon I_\circ R_\mathrm{e} \times \widetilde{\psi}_m(s)$, where G is the gravitational constant. Unfortunately $\widetilde{\psi}_m(s)$ cannot be expressed in terms of elementary functions, but, at variance with the density, for $r = 0$ it converges for all m:

$$\widetilde{\psi}_m(0) = \frac{4\Gamma(1+m)}{b^m}, \tag{7}$$

[Eq. (P12)].

3. The DF for anisotropic $R^{1/m}$ models

For any collisionless stationary system the DF f depends on the phase-space coordinates only through the isolating integrals of motion admitted by the underlying potential (*Jeans Theorem*, Chandrasekhar 1942), and moreover, if the system is also spherically symmetric in all its properties, f depends only on the binding energy and on the angular momentum square modulus L^2. Usually, the negative value of the binding energy, the *relative binding energy* $\mathscr{E}$, is used. For spherical models with $f = f(\mathscr{E}, L^2)$, the tangential components of the velocity dispersion tensor are identical, the only possible difference being between σ_r^2 and $\sigma_\theta^2 = \sigma_\phi^2 = \sigma_\mathrm{t}^2/2$, and the total velocity dispersion is $\sigma^2(r) = \sigma_\mathrm{r}^2(r) + \sigma_\mathrm{t}^2(r)$.

In the OM formulation the radially anisotropic case is obtained assuming a DF depending on $\mathscr{E}$ and L^2 only through the variable Q defined as:

$$Q = \mathscr{E} - \frac{L^2}{2r_{\rm a}^2}, \tag{8}$$

where $r_{\rm a}$ is the so-called *anisotropy radius*, and where $f(Q) \equiv 0$ for $Q < 0$. Under this assumption the models are characterized by radial anisotropy increasing with the galactic radius, and

$$\beta(r) \equiv 1 - \frac{\sigma_{\rm t}^2(r)}{2\sigma_{\rm r}^2(r)} = \frac{r^2}{r^2 + r_{\rm a}^2}. \tag{9}$$

In the limit $r_{\rm a} \to \infty$ the velocity dispersion tensor is globally isotropic. The simple relation between energy and angular momentum prescribed by Eq. (8) allows to express the DF as:

$$f(Q) = \frac{1}{\sqrt{8}\pi^2}\frac{d}{dQ}\int_0^Q \frac{d\varrho}{d\psi}\frac{d\psi}{\sqrt{Q-\psi}}, \tag{10}$$

where

$$\varrho(r) \equiv \left(1 + \frac{r^2}{r_{\rm a}^2}\right)\rho(r), \tag{11}$$

(BT, p.240). For ease of comparison we will use in the following $s_{\rm a} \equiv r_{\rm a}/R_{\rm e}$, and $f_m(Q) = [G^3\Upsilon I_\circ R_{\rm e}^5]^{-1/2} \times \widetilde{f}_m(\widetilde{Q})$, where $0 \le \widetilde{Q} \equiv Q/\psi_m(0) \le 1$.

3.1. Consistency

The basic requirement for any physically admissible DF is its non-negativity over the phase-space accessible to the system, and we call *consistent* any model with a nowhere negative f. The DF obtained by Eq. (10) is not automatically consistent, because the integral inversion does not guarantee its positivity, and so for any model one has to check the consistency: if for some positive value of Q it results $f < 0$, the adopted anisotropy radius is inconsistent with the assumed density profile. For example, in Paper I it was shown that globally isotropic $R^{1/m}$ models are consistent for all the explored values of m. It is therefore of interest to investigate here the consistency of the same family of models for various degrees of anisotropy. In Fig. 1 we plot $\widetilde{f}_m$ vs. $\widetilde{Q}$ in the case of global isotropy and strong anisotropy. A common characteristic is that the central divergence of the DFs, present in all globally isotropic models, is unaffected by OM anisotropy, a behaviour similar to that analytically discussed in Ciotti (1996), and for which the same qualitative explanation holds. This divergence – as for any density profile with total finite mass – is not a problem: although the central phase-space density of the models diverges, the corresponding mass does not. The requirement of consistency leads to define the critical anisotropy radius for consistency $(s_{\rm a})_{\rm c}$ so that for $s_{\rm a} < (s_{\rm a})_{\rm c}$ a *negative* DF for some admissible value of Q is obtained. The existence of a critical anisotropy radius for the $R^{1/m}$ models is easily understandable, remembering that a *completely* radial orbital distribution cannot be sustained by density profiles less

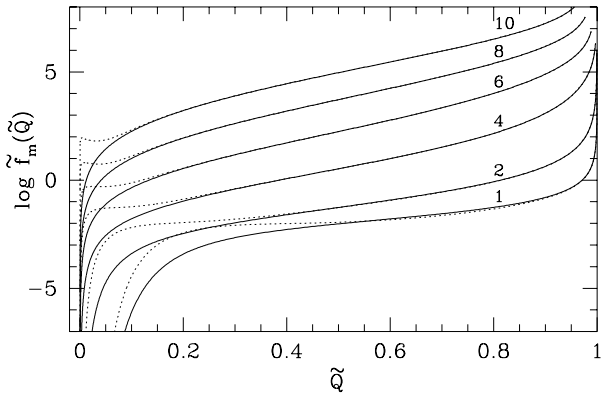

Fig. 1. The DFs for globally isotropic (solid lines) and stable anisotropic (ξ = 1.7, dotted lines) $R^{1/m}$ models.

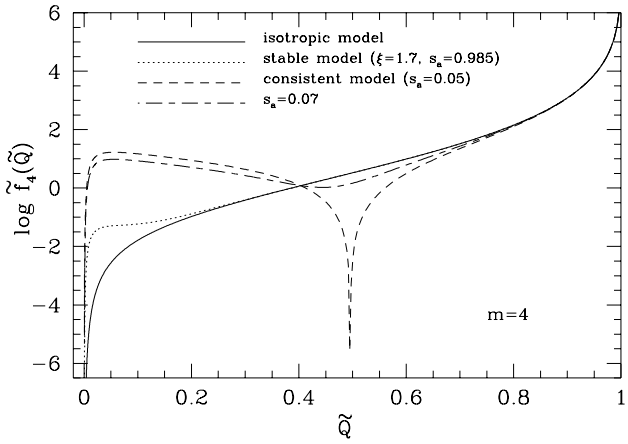

Fig. 2. The modifications of the de Vaucouleurs DF, moving from the globally isotropic case (solid line), to the ξ = 1.7 anisotropy (dotted line), and to the critical anisotropy for consistency (dashed line).

divergent than $1/r^2$ (see, e.g., Ciotti & Pellegrini 1992 for an easy proof), and that the logarithmic slope for $R^{1/m}$ models is $1/m - 1$ for $r \to 0$. It is then interesting to show in detail the effect of a decreasing $s_{\rm a}$ on the DF of $R^{1/m}$ models. In particular, in Fig. 2 we show the modifications on the de Vaucouleurs DF. Note that approaching $(s_{\rm a})_{\rm c}$ the DF becomes more and more depressed in the regions corresponding to intermediate values of the parameter $\widetilde{Q}$, i.e., $\widetilde{f}_4$ becomes first negative outside the center. The dramatic effect of the anisotropy when $s_{\rm a}$ is near its critical value is apparent in Fig. 2, where we have plotted $\widetilde{f}_4$ also for a slightly higher value of $s_{\rm a}$. This behaviour is common to the whole family of the $R^{1/m}$ models, and seems to be more a consequence of the OM parameterization itself than a characteristic of some specific mass model.[1]

In Fig. 3 (solid line) $(s_{\rm a})_{\rm c}$ is plotted in the parameter space $(m; s_{\rm a})$. Note how $(s_{\rm a})_{\rm c}$ asymptotically decreases towards very small values for increasing m. The qualitative trend of $(s_{\rm a})_{\rm c}$

[1] An identical behaviour it is found also for one and two component Hernquist models, discussed in Ciotti (1996).

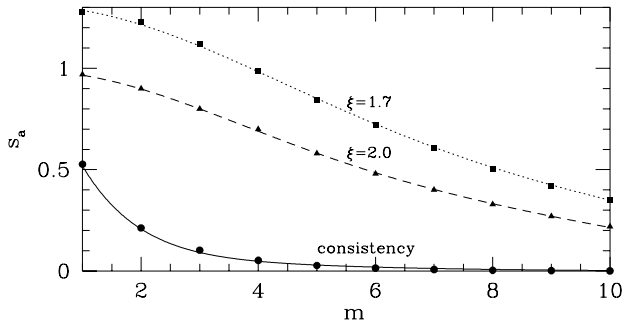

Fig. 3. The minimum value of the anisotropy radius for the model consistency (solid line), and that for the model stability, for two different values of ξ. The lines are the interpolating functions given in the text.

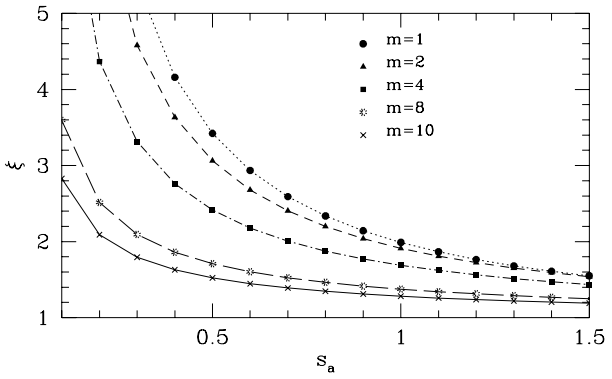

Fig. 4. The value of the stability parameter ξ for various m and for an increasing anisotropy radius.

Table 1. Critical values of s_a for consistency and stability in the cases ξ = 1.7 and ξ = 2, for integer values of m.

m	$(s_a)_c$	$(s_a)_{\xi=2}$	$(s_a)_{\xi=1.7}$
1	$5.3\,10^{-1}$	0.97	1.275
2	$2.1\,10^{-1}$	0.90	1.230
3	$1.0\,10^{-1}$	0.80	1.120
4	$5.3\,10^{-2}$	0.70	0.985
5	$2.7\,10^{-2}$	0.58	0.845
6	$1.5\,10^{-2}$	0.48	0.720
7	$7.7\,10^{-3}$	0.40	0.605
8	$4.1\,10^{-3}$	0.33	0.505
9	$2.1\,10^{-3}$	0.27	0.420
10	$1.1\,10^{-3}$	0.22	0.350

is due to the behaviour of $\widetilde{\nu}_m$: for small m this results in a quite flat density distribution, and so only "high" values for s_a are permitted; the opposite is true for high m models, for the density becomes more and more similar to a profile $\propto 1/r$, and a stronger radial anisotropy is admitted. The flattening of the curve $(s_a)_c$ for high m is explained by the same argument. As can be seen in Fig. 3, a good fit of $(s_a)_c$ as function of m is given by:

$$(s_a)_c \simeq e^{-0.93\,m}(1.32 - 9.85\,10^{-3}m^2 + 3.28\,10^{-3}m^4), \quad (12)$$

while the exact values are given for integer m in Table 1.

3.2. Stability

A given density model is not useful for applications on data-modelling if unstable. In Paper I it was shown in a rigorous way that globally isotropic $R^{1/m}$ models are stable. Unfortunately for anisotropic models the same approach is not possible, and so only approximate results can be obtained (unless one performs a much more complex linear stability analysis). Here, as in Carollo, de Zeeuw, & van der Marel (1995, hereafter CZM), the stability of anisotropic models is investigated in a semi-quantitative way using the radial-orbit instability indicator $\xi \equiv 2K_r/K_t$ (see, e.g., Fridman & Polyachenko, 1984), where $K_t = 2\pi \int \rho\sigma_t^2 r^2 dr$ and $K_r = 2\pi \int \rho\sigma_r^2 r^2 dr$ are the tangential and the radial kinetic energies, and have been numerically computed. This parameter is known to be a robust indicator, i.e., it is quite independent of the assumed density distribution profile, and when $\xi \gtrsim 1.5 \div 2$ the model is likely to be unstable. Note that for any globally isotropic model ξ = 1, because $2K_r = K_t$, while in presence of radial anisotropy $2K_r > K_t$, and so $\xi > 1$. For the investigated models $\xi = \xi(s_a, m)$, and for a fixed m it decreases towards unity for increasing s_a (see Fig. 4), according to the previous discussion. So, assuming a fiducial critical value of ξ for stability, a minimum value for the anisotropy radius $(s_a)_\xi$ is obtained, i.e., all models with $s_a < (s_a)_\xi$ are unstable (see also point 4 in Sect. 6).

In Fig. 3 $(s_a)_\xi$ is shown for two different ξ, and the corresponding values are given in Table 1. As it is intuitive, for each m, $(s_a)_\xi > (s_a)_c$: all models in the strip $(s_a)_c \le s_a \le (s_a)_\xi$ are consistent but unstable. As in the consistency analysis, also for stability an increase of m corresponds to a decrease in $(s_a)_\xi$: this is due to the fact that inside s_a the orbital distribution is nearly isotropic, and with increasing m a higher fraction of the mass is contained in the central regions of the model, thus exerting a more efficient stabilizing influence on the system (Polyachenko 1987). A fit of the minimum anisotropy radius for stability, as a function of m, and having assumed as stability requirement that ξ = 1.7, is

$$(s_a)_\xi \simeq e^{-0.019m^2}(1.31 - 3.17\,10^{-4}m^2 + 1.06\,10^{-4}m^4). \quad (13)$$

4. Velocity dispersion profiles

In this section we present the spatial and line–of–sight velocity dispersions profiles for the $R^{1/m}$ models with radial orbital anisotropy, and we compare them with the analogous globally isotropic cases, fully described in Paper I. In order to obtain the radial component $\sigma_r(r)$, we integrate the Jeans equation

$$\frac{1}{\rho(r)}\frac{d\rho(r)\sigma_r^2(r)}{dr} + 2\frac{\beta(r)\sigma_r^2(r)}{r} = \frac{d\psi(r)}{dr}, \quad (14)$$

with the natural boundary condition $\rho\sigma_r^2 \to 0$ for $r \to \infty$. Having assumed OM anisotropy, the integral solution can be written explicitly, as shown by Binney & Mamon (1982), and after normalization $\sigma_r^2(r) = G\Upsilon I_\circ R_e \times \tilde{\sigma}_r^2(s)$. The tangential velocity dispersion is then obtained from Eq. (9). In Fig. 5, σ_r/σ_V and σ_θ/σ_V are shown for some values of m, where $\sigma_V^2 = (2\pi/M)\int_0^\infty \rho\psi r^2 dr$, is the virial velocity dispersion. After normalization it results that a very good fit is given by

$$\tilde{\sigma}_V^2 \simeq 4.7 e^{-1.82\,m}. \quad (15)$$

A common feature of all the models is the characteristic central depression of the velocity dispersion profiles: the explanation of this behaviour for isotropic models was qualitatively given by Binney (1980) for the de Vaucouleurs law, and analytically for all the $R^{1/m}$ models in Paper I. We note that with increasing m the maximum moves towards smaller and smaller radii (for the $m = 10$ model the maximum is inside $s = 10^{-2}$), and its value becomes correspondingly higher and higher. The same behaviour is shown also in the strongly *anisotropic* models, both in σ_r and σ_t. It can be noted how the position and the value of the maximum are not strongly affected by anisotropy.

4.1. Projected and aperture velocity dispersions

More important for observational purposes is the line–of–sight (or projected) velocity dispersion profile $\sigma_P(R)$, obtained from σ_r as:

$$I(R)\sigma_P^2(R) = 2\int_R^\infty \left[1 - \beta(r)\frac{R^2}{r^2}\right] \frac{\nu(r)\sigma_r^2(r) r dr}{\sqrt{r^2 - R^2}}, \quad (16)$$

(see, e.g., BT, p. 208).

In Fig. 6 σ_P/σ_V corresponding to the same models described in Fig. 5 is shown. Note that, as a consequence of projection, the central depression is somewhat reduced but does not completely disappear. We give here a simple approximation of the position of the maximum and its height, as a function of m, in the case of global isotropy:

$$\left(\frac{\sigma_P}{\sigma_V}\right)_{Max} \simeq 0.62\, e^{0.07\,m}, \quad (17)$$

$$\frac{R_{Max}}{R_e} \simeq e^{-0.13m^2}(0.36 - 2.27\,10^{-3}m^2 + 7.58\,10^{-4}m^4). \quad (18)$$

These fitting formulae may be useful when correcting the observed values of the velocity dispersion, in simple applications of the virial theorem.

When observed through an aperture of finite size, the projected velocity dispersion profile is weighted on the brightness profile $I(R)$. As in Ciotti et al. (1996), we approximate this quantity calculating the *aperture* velocity dispersion, defined as

$$LP(R)\sigma_a^2(R) = 2\pi\int_0^R I(R')\sigma_P^2(R')R'\, dR', \quad (19)$$

where $LP(R)$ is the projected luminosity inside R [Eq. (P3)]. In Fig. 7 we plot $\sigma_a(R)/\sigma_V$ for the same models of Fig. 5. Note how, independently of the anisotropy radius, $\sigma_a \to \sigma_V/\sqrt{3}$ for $R \to \infty$: this result can be proved to be true for *any* assumed anisotropy (see, e.g., Ciotti 1994).

4.2. Implications on the FP

Looking at our results on the velocity dispersion profiles, we are tempted to discuss qualitatively their implications on the problem of the FP tilt and thickness.

Two main considerations can be made. The first concerns the effect of radial anisotropy as a possible origin of the FP tilt, through a systematic increase of it with galaxy luminosity. From Fig. 7, where the maximum degree of (OM) anisotropy consistent with stability is considered, it is clear that the radial anisotropy cannot produce – in the assumption of structural homology (i.e., the same m for all galaxies) – the required variation of a factor of 3 in the observed squared velocity dispersion. This conclusion was already reached for different galaxy models in Ciotti et al. (1996). In any case – at least in principle – a possible observational test for the importance of anisotropy would be to construct the FP using σ_a measured at large radii, and see whether its tilt is reduced.

The second point concerns the problem of the very small thickness of the FP. From Fig. 7 one can see that for increasing m the maximum deviation between the isotropic and anisotropic velocity dispersions becomes smaller and smaller: for example, the percentage difference of their squared values for $m = 2$ is $\simeq 15\%$, for $m = 4$ it is already reduced to $\simeq 7\%$, and for $m = 10$ is less than 6%. This implies that the anisotropy is not required to be fine-tuned with the galaxy luminosity in order to maintain the small observed FP scatter ($< 12\%$ in σ_a^2; see, Ciotti et al. 1996); on the contrary, all the admissible anisotropies can be present at each luminosity maintaining at the same time the FP thin.

5. Velocity profiles

The velocity profile (VP) at a certain projected distance from the galaxy center is the distribution of the stars line–of–sight velocities at that point. It is strictly linked to the line profile in the observed spectrum, that is the convolution of the stellar spectra with a certain VP. The shape of the VPs depends not only on the galactic potential, but also on the stars orbital distribution, a dynamical property not fully determined by the galactic potential itself. That is why the usual assumption of a gaussian shape for the VPs can generate a loss of information, and for this reason it has been suggested that the analysis of the deviations of VPs from gaussianity may give important insights on the dynamical structure of a galaxy (van der Marel 1994).

In the case of OM anisotropy the VPs can be numerically recovered from the $f(Q)$ using the integral expression given by CZM. As usual, we expand the VPs on the Gauss-Hermite basis:

$$VP(v) = \frac{\gamma\, e^{\frac{-v^2}{2\sigma^2}}}{\sqrt{2\pi}\,\sigma}\sum_{j=0}^{N} h_j\, H_j(v/\sigma), \quad (20)$$

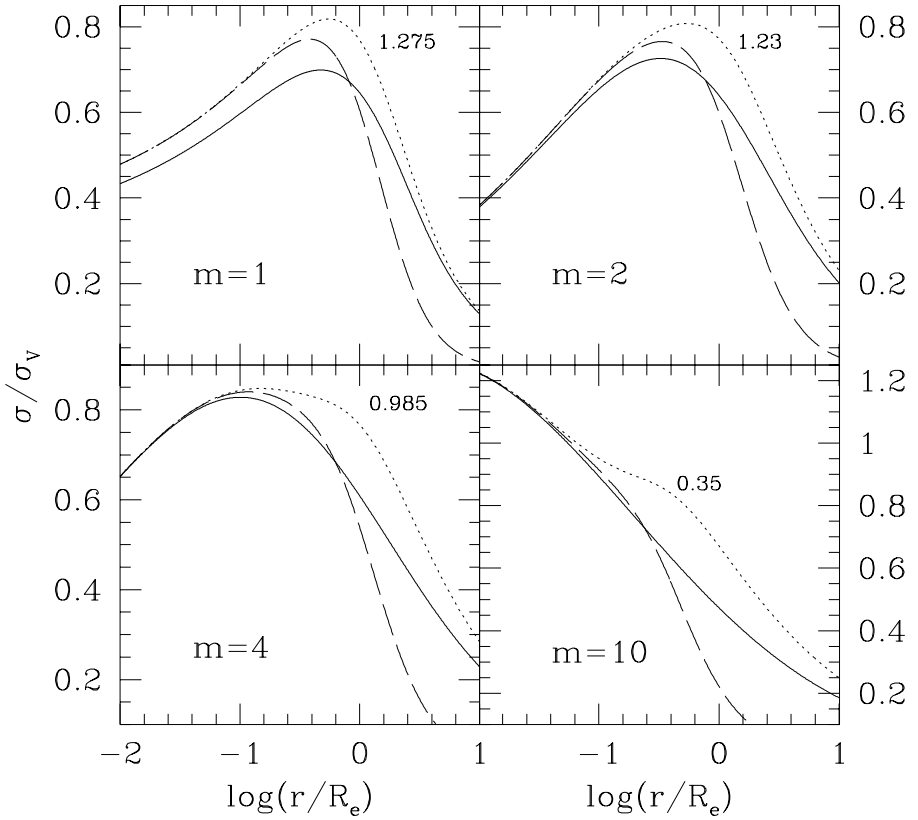

Fig. 5. The isotropic (solid lines), radial (dotted lines), and one-dimensional tangential (dashed lines) velocity dispersion profiles for various m and anisotropy radii. For each model the s_a is assumed to be the minimum possible for stability (with ξ = 1.7), and its value is the number printed in each panel.

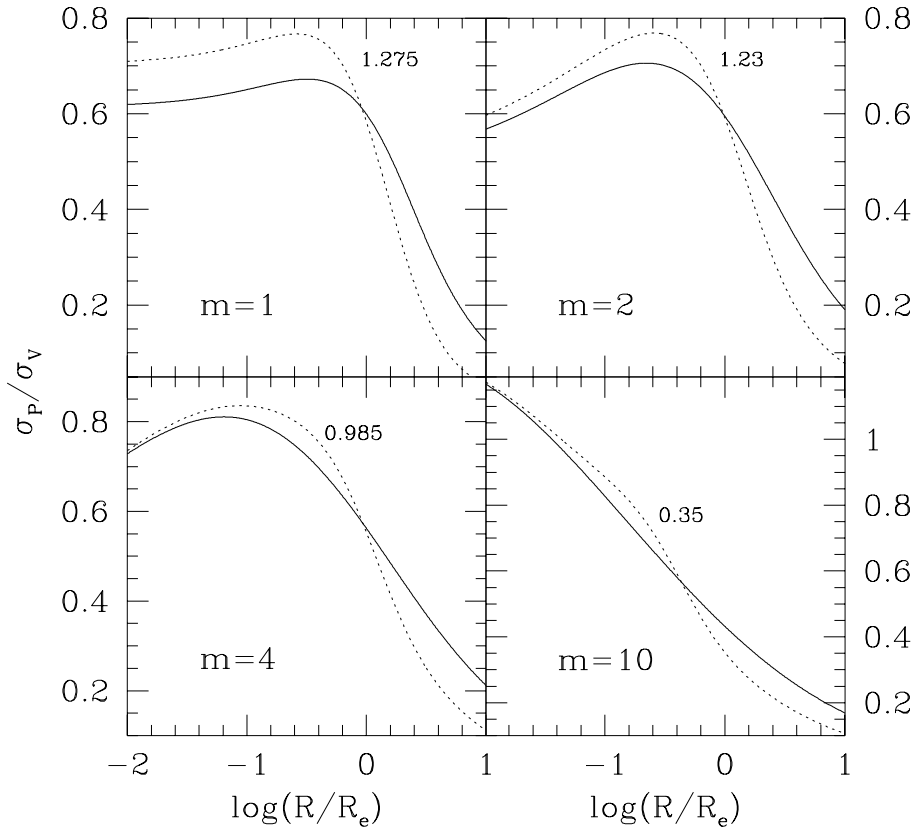

Fig. 6. The projected velocity dispersion for the same models shown in Fig. 5. The solid line refers to the globally isotropic models, and the dotted line to the anisotropic ones.

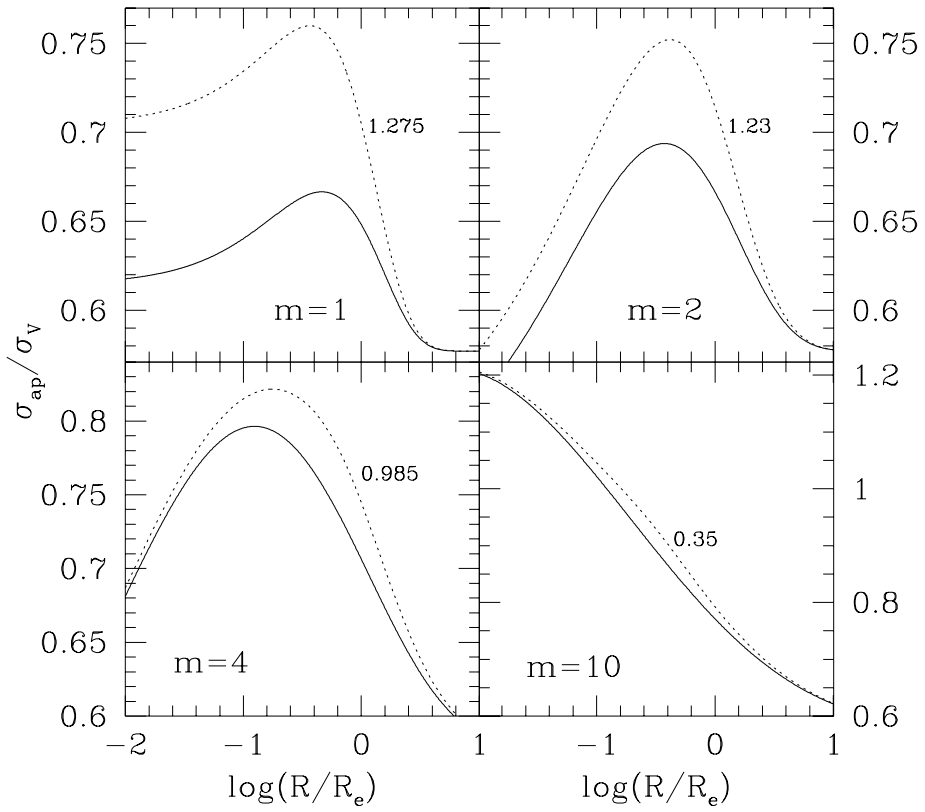

Fig. 7. The aperture velocity dispersion for the same models shown in Fig. 5. The solid line refers to the globally isotropic models, and the dotted line to the anisotropic ones.

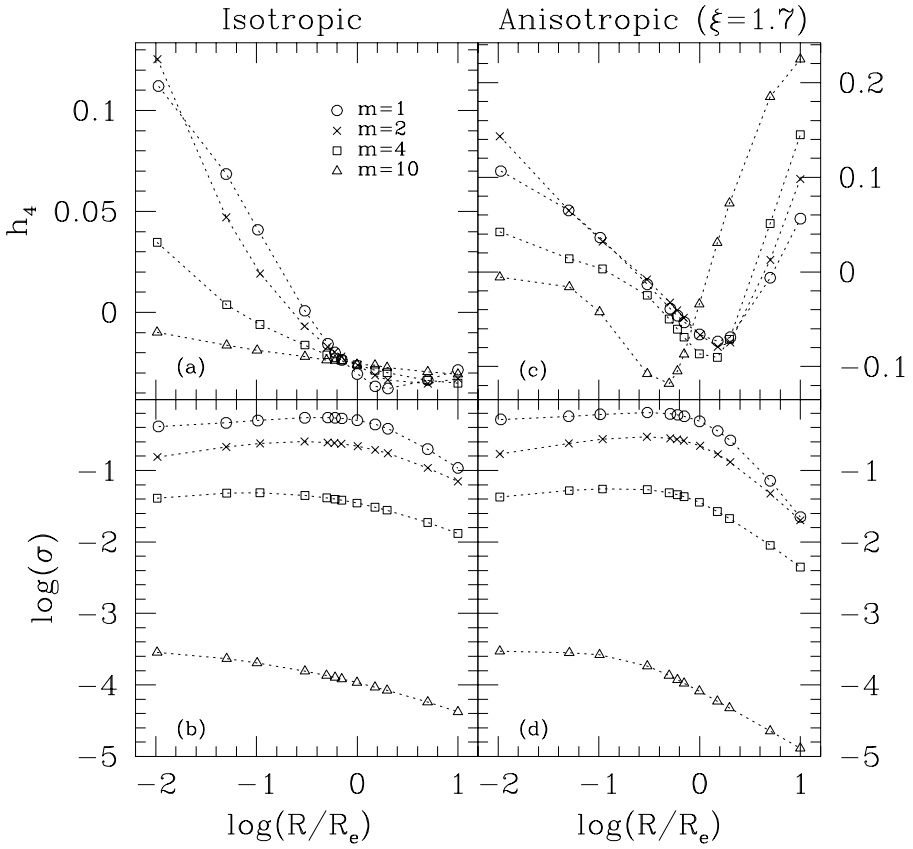

Fig. 8a–d. The values of the parameters h_4 (upper panels) and σ (normalized to $(G\Upsilon I_\circ R_e)^{1/2}$, lower panels) characterizing the VPs of the $R^{1/m}$ models, as a function of R, for m = 1 (circles), m = 2 (crosses), m = 4 (squares), and m = 10 (triangles). Left panels refer to the isotropic models, right panels to anisotropic (ξ = 1.7) models.

(Gerhard 1993, van der Marel & Franx 1993), where the H_j are the Hermite polynomials as given in van der Marel & Franx. The even coefficients h_{2j} measure symmetric deviations from a pure gaussian, while the odd coefficients h_{2j+1} are identically zero for our models because the DF depends only on L^2. We limit our investigation to the coefficient h_4, because higher order coefficients are usually not available from spectroscopic observations. The uncertainties in the published data on h_4 are of the order of ~ 0.02 (CZM). In practice, we fix $h_0 = 1$, and $h_2 = 0$ in Eq. (20), thus requiring that the first term is the best-fitting gaussian, and we minimize the χ^2 using the Levenberg–Marquardt method (*Numerical Recipes*, p.678) for the simultaneous non linear fit of (γ, σ, h_4). In Fig. 8 the radial behaviour of σ and h_4 for various m and for isotropic (left panels) and anisotropic ($\xi = 1.7$, right panels) models are shown.

Isotropic $R^{1/m}$ models have surprisingly gaussian VPs, as the smallness of their h_4 indicates (Fig. 8a). Exception is made by the low-m models, which present strongly non–gaussian VPs at small radii. Note also how, for $R \gtrsim 0.7 R_e$ the h_4 are completely indistinguishable for all m and indicate (slightly) flat-topped VPs (as generally a negative h_4 indicates). Moving inside, the differences between models become more and more important, but the global trend is towards VPs more peaked than the best-fitting gaussian, especially for low values of m. The radial behaviour of the corresponding dispersions σ of the best-fitting gaussian is shown in Fig. 8b, where the similarity (apart a re-scaling) with the dispersions plotted in Fig. 6 is evident.

For anisotropic models the σ (Fig. 8d) are very similar to that of the isotropic case, while the situation is quite different for the h_4 (Fig. 8c). Their values systematically decrease with radius in the inner regions, but rapidly increase at large radii, indicating significantly top–peaked VPs. This general trend, and the values as well, are nearly the same as those found by CZM for the γ models, and are due to the orbital distribution in the outer part of models with OM radial anisotropy.

Because of the differences in the trend of h_4 between the isotropic and the anisotropic cases, and because of the growing evidence that $R^{1/m}$-law appropriately describe the surface brightness profiles of elliptical galaxies, we conclude that a detailed study of the VPs along the FP could be in principle a tool to study the effect of orbital anisotropy on its tilt and thickness.

6. Conclusions

The results of this work are the following:

1. For OM anisotropic $R^{1/m}$ systems the consistency region in the parameter space is explored, and the minimum anisotropy radius that can be assumed for given m in order to have a physical model is determined. We find that models with high m can sustain more anisotropy than models with low m. A fit of the critical anisotropy radius for consistency is given.
2. The maximum anisotropy tolerated by $R^{1/m}$ models in order to be stable against radial orbit instability is approximately derived, with the aid of the standard stability parameter ξ. As expected, in this case the limitation on s_a is stronger than that required by consistency. Again, high-m models are more stable than low m models. A fit of the minimum anisotropy radius permitted for stability is given.
3. The spatial, projected, and aperture velocity dispersions are derived for various degrees of anisotropy. Their main characteristic is the fact that the off-center maximum – a feature already known and discussed for globally isotropic $R^{1/m}$ models – is still present, and not very much affected even by a strong anisotropy.
4. The implications of this work for the problem of the tilt and thickness of the FP of elliptical galaxies are that orbital anisotropy cannot be at the origin of the tilt if galaxies are described by the $R^{1/m}$ law and characterized by structural homology. At the same time, the small thickness of the FP at fixed luminosity does not require any fine tuning between anisotropy and luminosity, due to the stability requirement. We note that the Saha (1991, 1992) works on stability further strengthen our conclusions: he found that radial orbit instability can affect also models with ξ *smaller* than the values suggested by Fridman & Polyachenko (1984) and here used, and so a still smaller amount of anisotropy would be permitted.
5. The VPs are studied at various distances from the center for different anisotropy degrees and values of m. For globally isotropic models the VPs are very well approximated by a gaussian, except for very small radii and for low m, where detectable deviations from a pure gaussian are revealed. The lower order correction, parameterized by the coefficient h_4, shows that outside R_e the VPs are flat–topped and essentially indistinguishable for different values of m. On the contrary, the VPs of anisotropic models at $R \gtrsim R_e$ are more centrally peaked than a gaussian, and the values of h_4 increase with increasing m.

Acknowledgements. We would like to thank George Djorgovski for discussions, Roeland van der Marel for comments and Silvia Pellegrini for a careful reading of the manuscript. Also the anonymous referee is acknowledged for useful comments that improved the presentation of the paper. This work has been partially supported by the Italian MURST.

References

Andredakis Y.C., Peletier R.F., Balcells M., 1995, MNRAS, 275, 874
Bender R., Burstein D., Faber S.M., 1992, ApJ, 399, 380
Binney, J.J., 1980, MNRAS, 190, 873
Binney J.J., Mamon G.A., 1982, MNRAS, 200, 361
Binney J.J., Tremaine S., 1987, Galactic Dynamics, Princeton University Press, Princeton (BT)
Byun Y.I., Grillmair C., Faber S.M., Ajhar E.A., Dressler A., Kormendy J., Lauer T.R., Richstone D.O., Tremaine S.D., 1996, AJ, in press
Caon N., Capaccioli M., D'Onofrio M., 1993, MNRAS, 265, 1013
Capaccioli M., 1989, in The World of Galaxies, eds. H.G. Corwin and L. Bottinelli, Springer-Verlag, Berlin
Carollo C.M., de Zeeuw P.T., van der Marel R.P., 1995, MNRAS, 276, 1131 (CZM)
Chandrasekhar S., 1942, Principles of Stellar Dynamics, Chicago University Press, Chicago

Ciotti L., 1991, A&A, 249, 99 (Paper I)
Ciotti L., 1994, Cel. Mech. & Dyn. Astron., 60, 401
Ciotti L., 1996, ApJ, in press (November 1 issue)
Ciotti L., Pellegrini S., 1992, MNRAS, 255, 561
Ciotti L., Lanzoni B., Renzini, A., 1996, MNRAS, 282, 1
Ciotti L., Lanzoni B., 1996, in preparation (Paper III)
Courteau S., de Jong R.S., Broeils A.H., 1996, ApJL, 457, L1
Crane P., et al., 1993, AJ, 106, 1371
Davies J.I., Phillips S., Cawson M.G.M., Disney M.J., Kibblewhite E.J., 1988, MNRAS, 232, 239
de Vaucouleurs G., 1948, Ann. d'Astroph., 11, 247
de Zeeuw P.T., Carollo C.M., 1996 IAU Symposium 171, New Light on Galaxy Evolution, eds. R. Bender and R.L. Davies, Dordrecht: Kluwer
Djorgovski S., Davis M., 1987, ApJ, 313, 59
Dressler A., Lynden-Bell D., Burstein D., Davies R.L., Faber S.M., Terlevich R.J., Wegner G., 1987, ApJ, 313, 42
Erdély A., Magnus W., Oberhettinger F., Tricomi F.G., 1953, Higher transcendental functions, McGraw-Hill Book Company, Inc. (EMOT)
Ferrarese L., van den Bosch F.C., Ford H.C., Jaffe W., O'Connell R.W., 1994, AJ, 108, 1598
Fridman A.M., Polyachenko V.L., 1984, Physics of Gravitating Systems, 2 vols. New York: Springer
Gerhard O.E., 1993, MNRAS, 265, 213
Graham A., Lauer T.R., Colless M., Postman M., 1996, ApJ, 465, 534
Graham A., Colless M., 1996, preprint
Hjorth J., Madsen J., 1991, MNRAS, 253, 703
Jaffe W., Ford H.C., O'Connell R.W., van den Bosch F.C., Ferrarese L., 1994, AJ, 108, 1567
Kormendy J., Byun Y.I., Ajhar E.A., Lauer T.R., Dressler A., Faber S.M., Grillmair C., Gebhart K., Richstone D.O., Tremaine S.D., 1995, IAU Symposium 171: New Light on Galaxy Evolution, p. 105, eds. R. Bender and R.L. Davies, Dordrecht: Kluwer
Lauer T.R., Ajhar E.A., Byun Y.I., Dressler A., Faber S.M., Grillmair C., Kormendy J., Richstone D.O., Tremaine S.D., 1995, AJ, 110, 2622
Makino J., Akiyama K., Sugimoto D., 1990, Publ. Astron. Soc. Japan, 42, 205
Merritt D., 1985, AJ, 90, 1027
Møller P., Stiavelli M., Zeilinger W.W., 1995, MNRAS, 276, 979
Osipkov L.P., 1979, Pis'ma Astron.Zh., 5, 77
Polyachenko V.L., 1987, IAU Symposium 127: Structure and Dynamics of Elliptical Galaxies, p. 301, ed. P.T. de Zeeuw, Dordrecht, Reidel
Press W.H., Teukolsky S.A., Vetterling W.T., Flannery B.P., 1992, Numerical Recipes in Fortran, Second Edition, Cambridge University Press
Saha P., 1991, MNRAS, 248, 494
Saha P., 1992, MNRAS, 254, 132
Sersic J.L., 1968, Atlas de Galaxias Australes, Cordoba: Observatorio Astronomico
van der Marel R.P., Franx M., 1993, ApJ, 407, 525
van der Marel R.P., Ph.D. Thesis, 1994
Young C.K., Currie M.J., 1994, MNRAS, 268, L11

This article was processed by the author using Springer-Verlag LaTeX A&A style file *L-AA* version 3.